Inorganic Chemistry Communications 170 (2024) 113499

Contents lists available at ScienceDirect

Inorganic Chemistry Communications

journal homepage: www.elsevier.com/locate/inoche

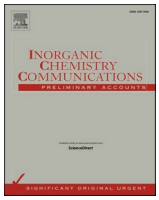

Research Article

Synthesis of Chitosan-Agar immobilized NiO-MgO bionanocomposites and their photocatalytic application towards toxic azo dye

Akshara Bassi [a], Parvathalu Kalakonda [b], Imran Hasan [c,*]

[a] Environmental Research Lab, Department of Chemistry, Chandigarh University, Mohali, Punjab 140413, India
[b] Dept of Physics, Smart Nano Materials Research Laboratory, Government City PG College Autonomous, Osmania University, Hyderabad Telangana 50002, India
[c] Department of Chemistry, College of Science, King Saud University, Riyadh 11451, Saudi Arabia

ARTICLE INFO

Keywords:
MgO-NiO Nanoparticles
Bionanocomposite
Methyl Orange
Biopolymer
Photocatalysis

ABSTRACT

In this study, NiO-MgO nanoparticles (NiMg NPs) were synthesized and incorporated into a biopolymer blend of chitosan (CTS) and agar agar gum (AA), forming the novel CTAG@NiMg bionanocomposite (BNC). Structural analysis revealed a crystal size of 19 nm and a direct band gap of 2.75 eV, indicating strong potential as a UV-active photocatalyst. TEM images confirmed uniform nanoparticle distribution with an average size of 25 nm. The elemental composition, verified by EDX spectra, showed weight percentages of C (21.32 %), O (31.47 %), Ni (35.39 %), and Mg (11.82 %). The CTAG@NiMg BNC demonstrated outstanding photocatalytic degradation of methyl orange (MO) dye, achieving 99.52 % degradation at pH 4 with 20-ppm concentration after 60 min under UV irradiation. The degradation followed pseudo-first-order kinetics, with rate constants (k_1) ranging from 0.011 to 0.030 min^{-1}, and a minimum half-life of 25.8 min at 15 ppm. Hydroxyl radicals (•OH) were identified as the primary reactive species driving the photocatalytic process. The material exhibited excellent reusability, retaining high degradation efficiency over four cycles. Compared to similar photocatalysts, CTAG@NiMg BNC demonstrated superior performance, faster degradation rates, and greater stability. Its enhanced surface area and porosity, as confirmed by BET analysis, contributed to better dye adsorption and faster reaction times. These properties make the CTAG@NiMg BNC a highly efficient, sustainable, and recyclable photocatalyst for environmental remediation, particularly in treating organic pollutants like methyl orange from aqueous solutions.

1. Introduction

Dyes are unwanted organic materials causing contamination of aquatic environment due to their toxicity, discoloration and extensively used in textile industries [1,74,85]. Methyl orange (MO) is anionic azo dye with chemical formula ($C_{14}H_{14}N_3NaO_3S$), extensively used in food, textile, pharmaceutical and leather industries and used as colouring agent to determines the presence of hydrogen chlorides and hydrogen gas [2,3,80]. MO is water-soluble, non-biodegradable and toxic which produces amines by reduction of azo linkage, it is carcinogenic, mutagenic and affect the biological ecosystem [3,4,83]. The azo and quinoid structure of MO in alkaline and acidic medium, MO cause serious health problems like seizures, joint and muscle pain, diarrhoea, irregularity in heartbeat, nausea, and ulceration of skin [5–7]. Also, MO present in water bodies inhibits penetration of sunlight and reduce photosynthesis which cause severe toxicity in aquatic life [8]. Thus, our prior task is to remove harmful dyes present in wastewater.

In literature, many several physiochemical and biological methods used to removes the different dyes from the wastewater [9–11]. Out of these methods, photocatalytic degradation is most effective process of scavenging out the organic or inorganic pollutants present in the wastewater by degrading into non-toxic small entities such as NO_2, H_2O and CO_2 etc [12,13,79]. The basic mechanism of photocatalytic degradation explains that when light equal or above band gap value of photocatalyst falls on catalyst surface, generation of the photoexcited electrons and holes takes place on the catalyst surface [14–16]. The generated electron and holes involved in reduction and to form $^{\bullet}OH/^{\bullet}O_2^-$ radicals which have oxidizing power to degrade the dye molecules into non-toxic entities [17–19]).

Semiconductors based on transition metal oxides nanoparticles like TiO_2, CuO, ZnO etc have different properties such as electronic, optical, thermal, chemical, gas sensing and catalysis which are useful for the degradation of dyes [20–22]. Photocatalyst based semiconductors, developed so that charge separation property will be improve through

* Corresponding author.
E-mail address: iabdulateef@ksu.edu.sa (I. Hasan).

https://doi.org/10.1016/j.inoche.2024.113499
Received 16 September 2024; Received in revised form 24 October 2024; Accepted 4 November 2024
Available online 7 November 2024

the formation of the heterojunction because the synergistic effect can successfully improve the lifecycle of the photo generated electrons due to their improvement in charge separation to enhance the photocatalysis [23]. Metal oxides are modified (doped, composite and mixed) to enhance the properties which shows new trend of photocatalysis [82]. Bimetallic metal oxide-based semiconductors improve the properties of catalysis and surface area due to the presence of cationic dopants and conductivity and electron transfer rate [24,25]. Various bimetallic oxide NPs are used for the degradation of dyes by photocatalysis. In present study, MgO-NiO NPs are synthesized, NiO is p-type semiconductor having band gap value (3.6 eV) and shows chemical, physical, and optical properties having low cost, non-toxic, photostability and used in water splitting [26,27,28]. MgO shows wide band gap (7.2 eV) with cubic structure and shows different properties like high adsorption capacity, ease of production, high surface reactivity, non-toxic and shows different applications in electronic, plasma drug screens, photocatalysis and in treatment of water [29,30,31,32]. NiO-MgO nanocomposites have been used as catalysis due to their multi-functional properties, binding energies, large surface area and isoelectric stability of NiO and MgO NPs even though MgO stabilised the lattice oxygen sites of NiO [33,34]. MgO is chemical stable and NiO with low cytotoxicity and genotoxicity effects on human even at low concentration of less than 0.3 mg/mL are great attractive antibacterial agents integrated into chitosan. The nanocomposites formed using NiO-MgO with biopolymers like chitosan and agar agar results great stability with reduced side effects [35].

Biopolymers belongs to the class of carbohydrates and proteins which are highly rich in carboxyl and hydroxy groups, enabling the green route for the synthesis of nanocomposite providing the matrix as host and acting as crosslinkers concurrently. Chitosan (CTS) is cationic polysaccharide, composed of β-D-glucosamine and acyl β-D-glucosamine residues having 1,4-β-linkage [36]. It is extracted from chitin, biodegradable, non-toxic, biocompatible in nature and used as adsorbent in different dyes removal processes [38,78]. The presence of functional groups in chitosan provides number of chelating sites to metals ions so as to reduce them in nanocomposite and degrade the organic molecules in the presence of UV–Vis radiations [73]. Besides, rate of hydroxy group increases under the presence of radiation, chitosan was grafted with Agar Agar (AA) is polysaccharide, having gelation properties polymer derived from different red algae i.e., Gelidium and Gracilaria [39]. It is composed of agrose and agrosepectic components which are used in the formation of hydrogels [37]. It used in many industrial applications like biomedical, cosmetics, foods, pharmaceuticals and biomedical as it act as binding, gelling and suspension agent [40].

Despite extensive research on NiO, MgO, and other metal oxide-based photocatalysts, there remain certain gaps in terms of stability, reusability, and overall degradation efficiency when these materials are used in free nanoparticle form. Previous studies have often focused on individual metal oxides or simple composites without incorporating biopolymer supports, which limits their practical applicability in real-world wastewater treatment systems. The present work introduces a novel approach by synthesizing chitosan-agar immobilized NiO-MgO bionanocomposites. This hybrid material offers several advantages over previously reported systems such as unlike earlier works such as [41,42,8,43,44] that primarily utilize unsupported nanomaterials, the use of chitosan and agar as biopolymeric matrices provides enhanced stability and ease of recovery after the photocatalytic process, addressing one of the major challenges faced by previous studies. The combination of NiO and MgO in a bionanocomposite form exploits the synergistic photocatalytic effects of both metal oxides, which has not been fully explored in earlier publications. The dual oxide system potentially enhances the electron-hole separation efficiency, leading to superior photocatalytic activity. While earlier research has employed synthetic or non-biodegradable materials as supports or stabilizers, our work incorporates environmentally friendly and biodegradable polymers (chitosan and agar), making the system more sustainable and applicable for green chemistry approaches. So, by introducing a bionanocomposite system that integrates the photocatalytic properties of metal oxides with the biocompatibility of natural polymers, this study aims to overcome limitations of previously reported materials, paving the way for more efficient and sustainable wastewater treatment solutions.

2. Material

2.1. Chemicals used

Magnesium acetate tetrahydrate ($(CH_3COO)_2Mg{\cdot}4H_2O$) AR grade was purchased from Loba Chemie. Nickel nitrate ($Ni(NO_3)_2{\cdot}6H_2O$) was purchased from Qualikems Laboratory reagents. Chitosan (low molecular weight) was brought from Loba Chemie. Agar agar gum was brought from Qualikems Laboratory reagents. Sodium hydroxide (NaOH) was purchased from Loba Chemie. Methyl orange dye was brought from Loba Chemie. The 1000 mg/L stock solution of methyl orange solution was ready by adding precise amount of dye in 100 mL of deionised water. The salts and reagents were taken in appropriate amount and deionised water was used during the experiments.

2.2. Synthesis of CTAG@NiMg BNC

The synthesis of the bionanocomposite (CTAG@NiMg) was conducted via a green and eco-friendly approach using a combination of coprecipitation and sol–gel methods. Chitosan (CTS) and agar agar (AA) biopolymer blend served as both a matrix and a reducing agent for the incorporation of NiO-MgO nanoparticles [27]. A biopolymer blend of chitosan and agar agar was prepared by dissolving 3 g of chitosan (CTS) and 2 g of agar agar (AA) in 100 mL of deionized water. The mixture was stirred vigorously on a magnetic stirrer to ensure complete dissolution of the biopolymers, resulting in a homogenous solution. Separate solutions of metal salts were prepared to serve as precursors for the synthesis of NiO-MgO nanoparticles. For the magnesium source, a 1 M solution of magnesium acetate tetrahydrate [$(CH_3COO)_2Mg.4H_2O$] was prepared by dissolving the appropriate amount in deionized water. For the nickel source, a 2 M solution of nickel nitrate hexahydrate [$Ni(NO_3)_2.6H_2O$] was similarly prepared in deionized water. Both solutions were stirred until completely dissolved. The metal precursor solutions were added dropwise to the previously prepared chitosan-agar solution in a controlled manner. This step was carried out using a three-necked round-bottom flask (500 mL capacity) equipped with a magnetic stirrer to ensure continuous and uniform mixing of the components. To initiate the coprecipitation of the metal ions, a 25 % ammonia solution (NH_4OH) was slowly added to the reaction mixture. The addition of ammonia was carefully monitored, and the pH of the solution was maintained between 8 and 9. During this process, greenish-white precipitates began to form, indicating the successful coprecipitation of NiO and MgO nanoparticles within the biopolymer matrix. The reaction mixture was stirred continuously for 4 h at room temperature to allow sufficient time for the nanoparticles to grow and be uniformly distributed within the biopolymer matrix. After the aging period, the resulting precipitate was filtered using a Buchner funnel and washed thoroughly with deionized water 4–5 times to remove any residual impurities or unreacted precursors. The filtered product was then dried in a hot air oven at 60 °C for 5 h to remove any remaining moisture and to obtain the final CTAG@NiMg bionanocomposite powder.

2.3. Characterisation of CTAG@NiMg BNC

The synthesized bionanocomposite was characterized by using different analytical techniques to find out the structure, crystal, surface morphology and different bonding involved in the material. The bond formation and functional groups between NiO-MgO and CTS-Agar biopolymer blend were investigated using Fourier Transform Infrared

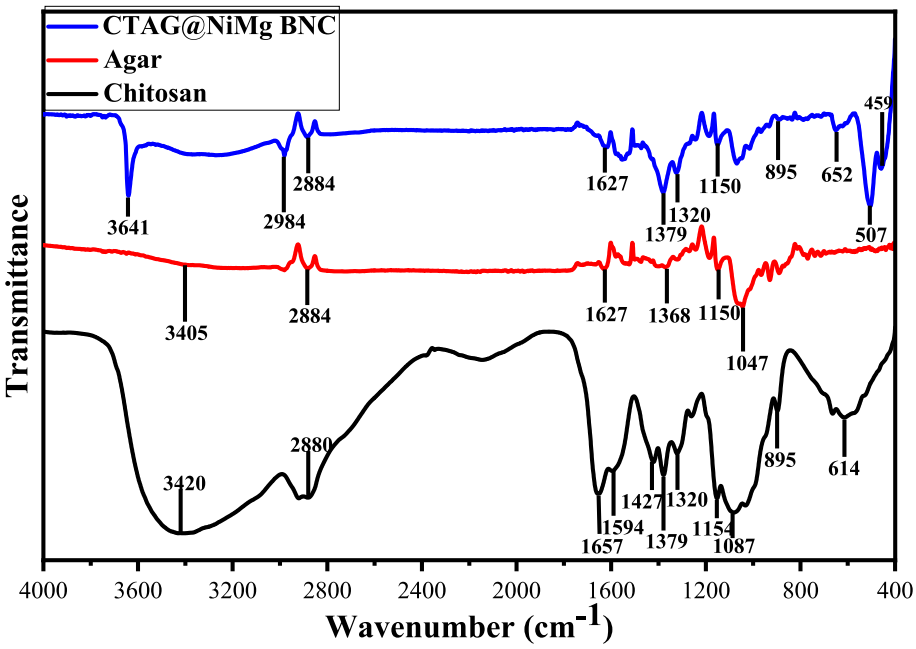

Fig. 1. FTIR spectra of chitosan (black line), agar (red line) and CTAG@NiMg BNC.

(FTIR) spectrophotometer Perkin Elmer (PE1600, USA) frequency having range from 400-4000 cm^{-1} with transmission mode. The information about structure and crystal lattice of NiO-MgO immobilized with CTS@Agar blend was investigated by Ultima X-ray Diffraction (XRD) (Rigaku, Tokyo, Japan). The surface morphology and composition of elements present in the material associated with Energy diffraction X-ray analysis (SEM-EDX) (SEM, JEOL GSM 6510LV, Japan). Transmission Electron Microscope (TEM, JEM 2100, Japan) was used to detect the particle size and its distribution in the CTS-Agar biopolymer blend. Selected area electron diffraction (SAED) method was performed with aperture at selected diameter of 200 nm at TEM section. The chemical composition and oxidation state of elements in material was evaluated by X-ray photoelectron spectroscopy (XPS, PHI 5000 Versa Probe II, FEI Inc.). The specific area of material was investigated on Micromeritics Tristar II and its and values were observed by Brunauer-Emmett-Teller method (BET). The Zetasizer advance (Malvern Panalytical) was employed to determine the dynamic size of material. The energy band gap, optical properties and concentration of MO dye photocatalytic activity before and after degradation was determined by using double beam UV–Vis spectrophotometer (Shimadzu UV-1900).

2.4. Photocatalytic experiment

First, the experiment was performed for different dyes with synthesised BNC material. Based on that experiment, results were obtained, it was found that MO dyes was showing more degradation and chosen for further experiments. The photocatalytic experiment was performed using continuous method with parameters like pH, MO concentration, dosage load and irradiation time under UV light (18 W, 254 nm). 20 mL of MO aliquot with different concentrations (5–30 ppm), pH (4,7 and

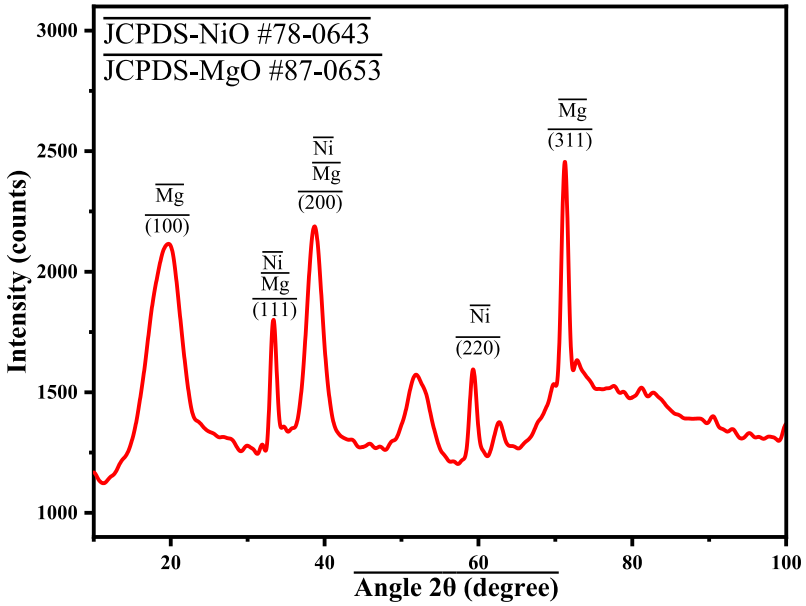

Fig. 2. XRD spectra of CTAG@NiMg BNC.

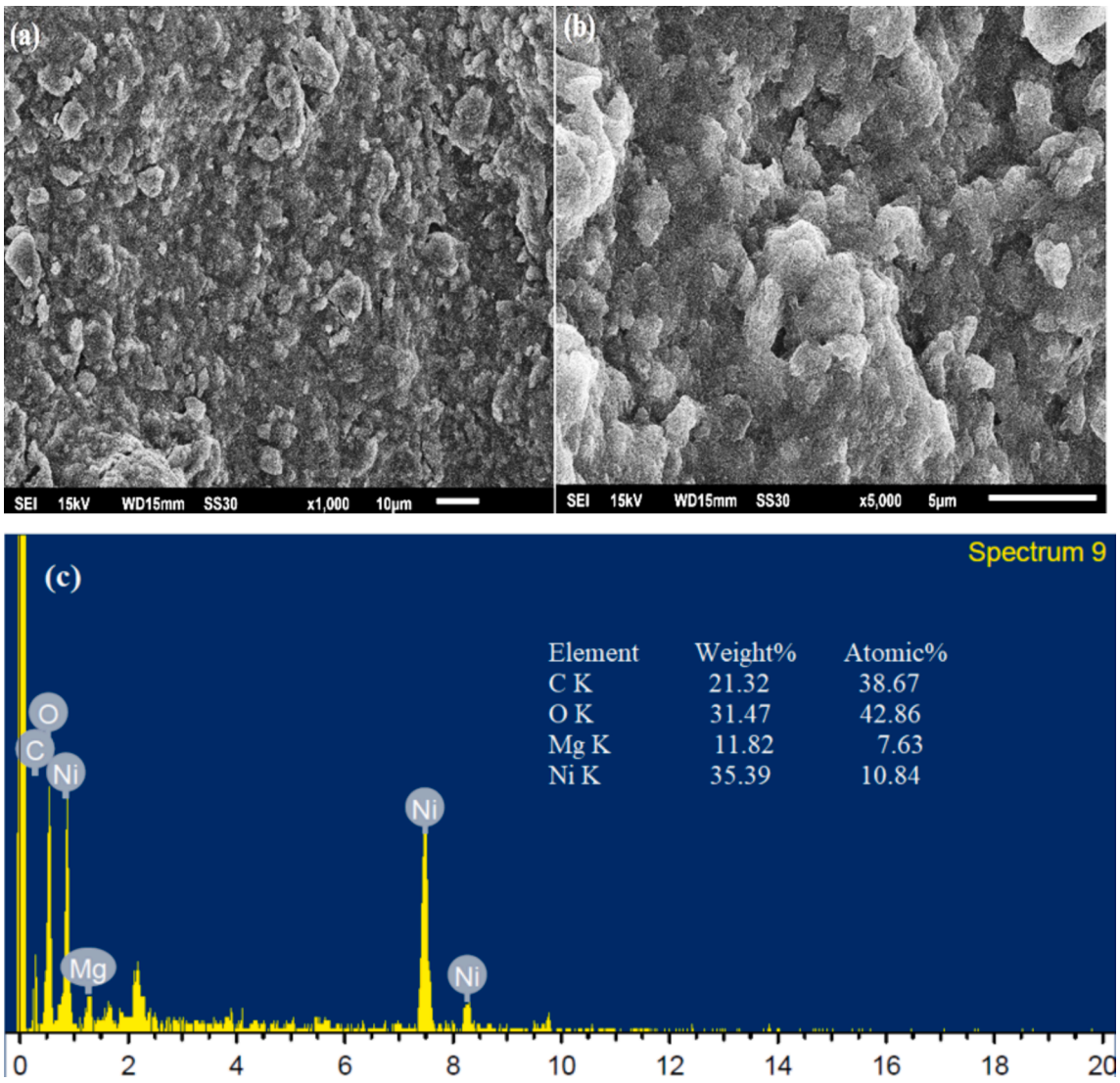

Fig. 3. (a, b) SEM image of CTS-Agar and CTAG@NiMg BNC, (c) EDX spectra with mapping of CTAG@NiMg BNC.

10), irradiation time (10–60 min) and dose load (10,15 and 20 mg). The efficiency of photocatalyst was analysed by amount of MO degraded in the aqueous solution. After the completion of reaction, MO effluents were collected and analysed by using UV–Vis spectrophotometer at λ_{max} = 464 nm and percentage degradation of MO dye was calculated by given equation-

$$\text{Photocatalytic Efficiency } (\%) = \frac{C_0 - C_e}{C_0} \times 100 \quad (1)$$

where C_0 and C_t are the initial and final concentration of MO dye respectively.

3. Results and Discussion

3.1. Characterisation of CTAG@NiMg BNC

Fig. 1 displays the FTIR spectra of CTS, Agar, and CTAG@NiMg BNC corresponds to vibration of specific functional groups. The FTIR spectra of chitosan (black line) examined absorption peaks at 3420 (O-H stretching overlapped with N-H stretching), 2880 (aliphatic $-CH_2$ stretching), 1657 (C = O stretching with amide-I confirm N-acetyl groups), 1594 (N-H bending of amide-II), 1427 (CH_2 bending), 1379 (symmetric CH_3 deformation), 1320 (C-N stretching of amide-III), 1154 (asymmetric bridged C-O-C), 1087 (C-O stretching) and 895 (C-N stretching) [45,46]. The FTIR spectra of agar (red line) shows peaks at 3405 (–OH stretching), 2884 (aliphatic –CH stretching), 1627 (C = O stretching), 1368 (C-OH stretching), 1150 and 1047 (C-O-C stretching) [47]). The FTIR spectra of CTAG@NiMg BNC shows all the characteristic absorption peaks from individual constituents with decreased intensity and new peaks at 2984 (R-N-C stretching between agar and chitosan), 652 (Ni-O stretching), 507 (Mg-O stretching) and 459 (confirms the formation Ni-O/Mg-O stretching) [33,48;49].

The XRD spectra of CTAG@NiMg BNC as shown in Fig. 2 which explains the crystalline structure and lattice information of synthesized nanocomposite. The peaks at 2Θ values of 19.7°, 33.3°, 38.7°, 59.4° and 71.2° corresponds to Miller indices values at (1 0 0), (1 1 1), (200), (220) and (311). From the literature, it was found that NiO-MgO NPs shows 2Θ values at 37.85, 41.98, 63.44, 74.83 and 78.00 corresponds to the Miller indices values at (1 1 1), (200), (220), (311) and (222) respectively [50,51,52]. On comparing the XRD spectra of synthesized BNC with literature data, it was found that NiO-MgO NPs are functionalized with CTS-Agar biopolymer. The results obtained of Miller indices values also support face cubic centred structure of NiO-MgO NPs. By using eq. (3), it was concluded that CTAG@NiMg BNC were 42 % crystalline and 58 % amorphous. The NC found to be more amorphous in nature because biopolymer matrix of CTS-Agar present which will covered the NiO-

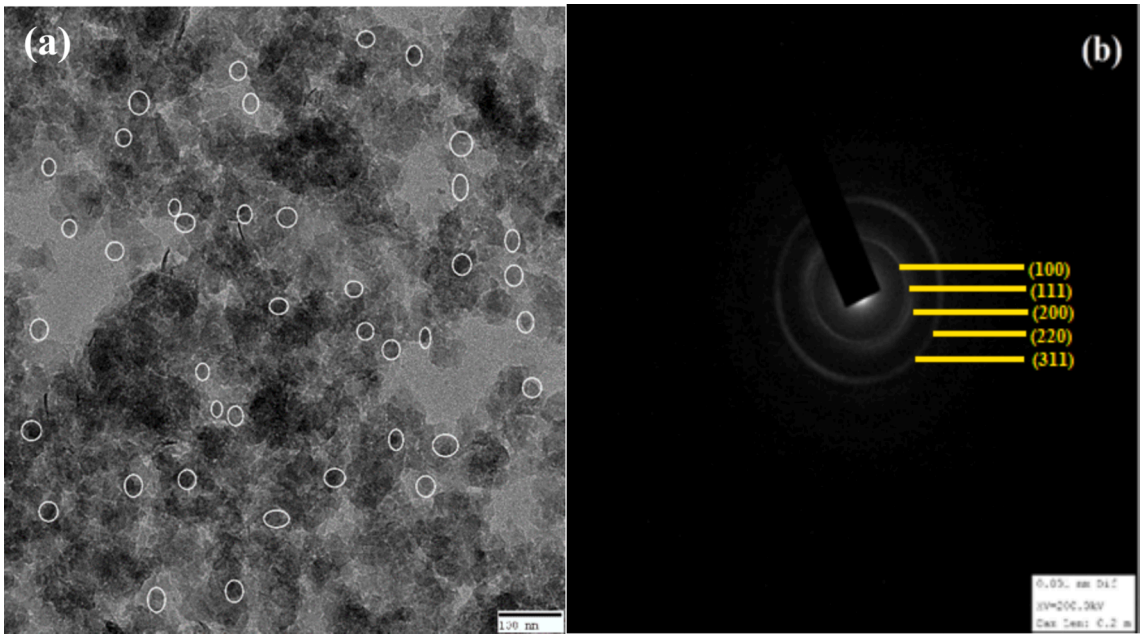

Fig. 4. (a, b) TEM and SAED image of CTAG@NiMg BNC respectively.

MgO NPs in the biopolymer matrix. The crystallite size and %crystalline can be calculated by using the equation given below. To calculate crystallite size, the equation is known as Scherrer Formula [75]

$$D = \frac{0.9\lambda}{\beta\cos\theta} \tag{2}$$

$$Crystallinity(\%) = \frac{AreaundertheCrystallinePeaks}{TotalArea} \times 100 \tag{3}$$

where, θ as diffraction angle, D as crystal size in nm, λ as wavelength (1.54 Å) and β as half width of peaks. By using Scherrer Equation, the crystal size of CTAG@NiMg BNC was found to be 19 nm.

The surface morphology of CTAG@NiMg BNC was observed by using SEM analysis. Fig. 3 (a) represents the SEM image of CTS-Agar biopolymer which are spherical in shaped. Fig. 3 (b) represents SEM image of CTAG@NiMg BNC which shows flaky structure due to the NiO-MgO are functionalized in the CTS-Agar biopolymer matrix. Fig. 3 (c) represents EDX spectra which shows elemental composition of the material having energy range of 1–20 keV. The weight percentage of each constituent in the material is C (21.32 %), O (31.47 %), Ni (35.39 %) and Mg (11.82). Further, the magnification of synthesized material as shown in Fig. S1 (a–e) shows the selected area SEM image with the distribution of elements C, O, Ni and Mg suggesting the material synthesized is pure and no foreign elements was found.

TEM analysis describes the size of particles and their distribution about biopolymer matrix with chemical homogeneity. TEM image of CTAG@NiMg BNC as shown in Fig. 4 (a) shows fine distribution of NiO-MgO in the biopolymer matrix of CTS-Agar with average particle size of 25 nm which is in close closeness with results obtained from XRD analysis. Fig. 4 (b) explains the SAED image of synthesized material found that each element is well distributed in the whole sample. In SAED, the diffraction peaks are matched with XRD pattern which proves that material is amorphous in nature.

The particle size is further supported by dynamic light scattering (DLS) analysis of the CTAG@NiMg BNC was done by using water as solvent. In Fig. S2, the experiment consists of three runs to obtained maximum extension of particles locality in the particle system. With 20–25 % of intensity, it was found that the average size was 23.5 nm. The size is bigger in hydrodynamic region because of the interaction of dispersant takes place in hydrodynamic diameter due to which exfoliation of CTS-Agar biopolymer in reaction occur.

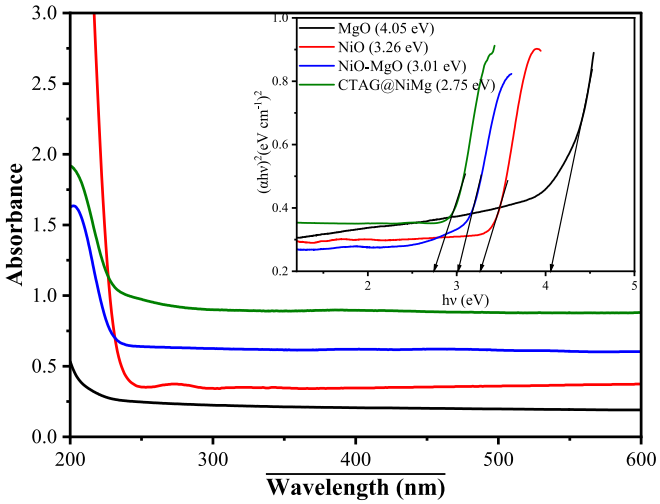

Fig. 5. UV spectra of CTAG@NiMg BNC and inserted is Tauc's plot of CTAG@NiMg BNC.

The band gap value and optical absorption of synthesized CTAG@-NiMg BNC and its constituents like MgO, NiO and NiO-MgO was estimated by using UV–Vis spectroscopy under range of wavelength from 200-800 nm. The indirect and direct band gap value of the CTAG@NiMg BNC was calculated by Tauc's plot and the equation given below [81]

$$\alpha h\nu = A(h\nu - E_g)^n \tag{4}$$

where, h = planks constant, v = frequency, α = coefficient of absorption, A = constant, n = constant for transition, for direct band n = 2 and for indirect band n = 1/2. Fig. 5 shows the UV spectra of MgO, NiO, NiO-MgO and CTAG@NiMg BNC. The UV absorption spectra for MgO NPs (black line) shows a very poor absorption near lower UV range from 200-300 nm wavelength and corresponding bandgap energy was found to be 4.05 eV which is in a range obtained by previous work [53]. The UV spectra of NiO NPs shows an absorption range from 250-350 nm with a energy bandgap of 3.26 eV which is also related with previous work

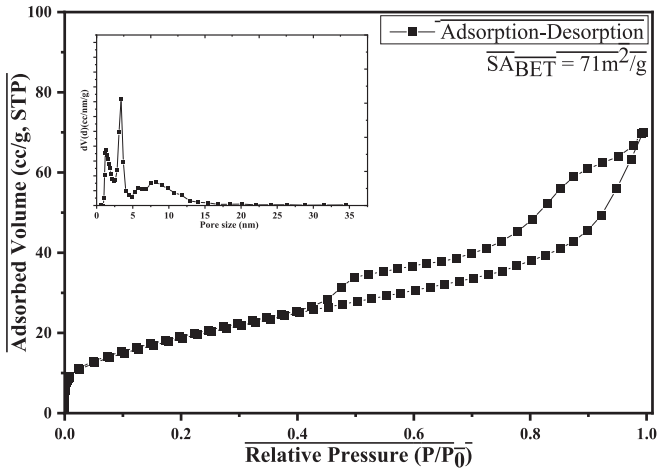

Fig. 6. N_2 Adsorption-desorption of CTAG@NiMg BNC by Barrett-Joyner-Halenda (BJH) pore size analysis graph.

[54]. The absorption spectra of NiO-MgO NPs shows a broader range of absorption from 250 to 350 nm corresponding to n-π* transitions which may be attributed to the excitation of surface O_2^- anions of NiO-MgO NPs [55,56]. The direct energy bandgap value was calculated as 3.01 eV. After surface functionalization of NiO-MgO with CTS-Agar, the resultant material CTAG@NiMg exhibited the absorption range (smaller magnitude) from 300 to 400 nm. This red shift in absorption spectra suggested that NiO-MgO NPs have been successfully stabilized and immobilized by CTS-Agar biopolymer blend. The direct energy bandgap value was found to be 2.75 eV suggested that immobilization resulted in reduction of bandgap and improving the photocatalytic activity.

At low temperature, the porosity and surface area for CTAG@NiMg BNC were examined by N_2 adsorption–desorption analysis. Fig. 6 shows the N_2 adsorption–desorption isotherm with pores size distribution by Barrett-Joyner-Halenda (BJH) displays type IV form with characteristics of mesoporous structure. The BET surface area for synthesized material was 71 m^2/g and pore size are 0.09 nm. From the literature, BET surface area for NiO NPs was 11.617 and 40.5 m^2/g whereas for MgO NPs was 41 and 67 m^2/g [57,58,59,60]. The BET surface area for NiO-MgO was found to be 56 m^2/g given in Fig. S3. So, based on the obtained results, it was found that the NiO-MgO NPs have been successfully distributed among the CTS-Agar biopolymer matrix and resulted in an enhanced value of surface area of 71 m^2/g.

The oxidation state and chemical composition of elements in the CTAG@NiMg BNC were analysed by X-ray photoelectron spectra (XPS) spectra. Fig. 7 (a) shows the survey scan of CTAG@NiMg BNC that explains the presence of carbon, oxygen, nickel, and magnesium. Fig. 7 (b) shows the binding energy peaks value at 283.1 eV (C–C/C–H), 287.3 eV (O-C = O) and 282.8 eV (C-O/C-N) represents chitosan and agar agar [61]. Fig. 7 (c) shows the binding energy peaks value at 528.9 eV, 527.9 eV and 523.3 eV reveal the three kinds of bonding i.e., O^{2-}, O–H and MgO–NiO respectively. Fig. 7 (d) shows the binding energy peak value at 47.7 eV corresponds to Mg^{2+} ions involve Mg $2p_{3/2}$ spin-orbital state [62]. Fig. 7 (e) shows the binding energy peak value at 86.3 eV corresponds to the linkage of Mg bonded with O contain groups in Mg2s [63]. Fig. 7 (f) shows the binding energy peak value at 871.3 eV and 853.5 eV corresponds to Ni$2p_{1/2}$ and Ni$2p_{3/2}$ respectively [64].

3.2. Photocatalytic experiment

3.2.1. Selectivity test

A selectivity test was performed using 10 mg of CTAG@NiMg BNC to evaluate its photocatalytic efficiency with various dyes, including bromophenol blue (BP), methyl orange (MO), Congo red (CR), malachite green (MG), crystal violet (CV), and methylene blue (MB). As shown in Fig. S4 (a, b), the synthesized CTAG@NiMg BNC demonstrated the highest photocatalytic sensitivity towards MO, achieving an efficiency of 99.51 % degradation under UV irradiation. This remarkable selectivity for MO suggests that the material has a strong affinity for this dye, likely due to favourable interactions between the dye molecules and the surface properties of the composite. The high efficiency in degrading MO may be attributed to the structural and electronic properties of both the dye and the photocatalyst. In contrast, the photocatalytic performance of CTAG@NiMg BNC with other dyes such as BP, CR, MG, CV, and MB was notably lower, indicating that the composite's active sites have a preferential affinity for MO. The variation in degradation efficiency among the different dyes is likely influenced by factors such as molecular size, structure, charge, and the nature of their interaction with the photocatalyst's surface. Given these results, subsequent photocatalytic experiments were focused on MO degradation to leverage the high selectivity and efficiency of CTAG@NiMg BNC with this particular dye.

3.2.2. Photocatalytic activity of CTAG@NiMg and its individual compounds

Photocatalytic experiments were conducted using 10 mg samples of NiO, MgO, NiO-MgO, and CTAG@NiMg BNC in the presence of 20 ppm MO dye, subjected to 60 min of UV light irradiation. The degradation results, as presented in Fig. S5 (a, b), reveal that NiO nanoparticles achieved a degradation efficiency of 73 %, while MgO nanoparticles showed 60 % degradation. The NiO-MgO composite demonstrated an enhanced degradation of 86 %, and the CTAG@NiMg BNC exhibited the highest efficiency, with 99.27 % MO dye degradation. Overall, the results highlight the critical role of material composition and surface modification in influencing photocatalytic efficiency. While NiO and MgO alone show moderate activity, their combination and subsequent modification with Ag and CTAB significantly enhance the photocatalytic performance, with the CTAG@NiMg BNC demonstrating almost complete dye degradation. This superior performance positions CTAG@NiMg BNC as a promising photocatalyst for environmental remediation applications.

3.2.3. Effect of leaching experiment

The experiments were designed to examine the removal of dyes in the presence of catalyst under UV light (photocatalysis), in presence of catalyst (adsorption) and in absence of catalyst under UV light (photolysis). The experiments were performed at pH 7, 5–30 ppm initial concentration, dosage load of 0.02 g/L at irradiation time of 30 min. Fig. 8 shows the %degradation of MO dye versus irradiation time. It was found that in the presence of catalyst under halogen lamp the degradation of dye increases with the increase irradiation time and removal yield was approximately 92 % was found after 30 min. However, in the case of light source alone in absence of catalyst (i.e., photolysis) the % degradation was found to be 15 % whereas in the presence of catalyst but no light source (i.e., adsorption) the %degradation was found to be 60 %. Form this experiment, it was concluded that the dye was only degraded in the presence of light source with catalyst i.e., photocatalysis is best method for dye degradation.

3.2.4. Effect of initial dye concentration

The effect of different concentration of MO on photocatalytic efficiency and %degradation of catalyst was investigate using 25 mL of aliquot of 5–30 ppm MO using 20 mg of catalyst dose under UV light. Fig. 9 (a, b) shows the results of different concentration of MO dye and concentration vs %degradation respectively. It was found that as the concentration increases from 5-30 mg/L but there was abnormal behaviour found in %degradation of MO was exhibited. By using UV–Vis curve, the %degradation of MO for different concentrations were- 5 ppm MO, 89.5 %; 10 ppm MO; 93.4 %, 15 ppm MO, 95.1 %; 20 ppm MO, 96.2 %; 25 ppm MO, 95 %; and 30 ppm MO 94.5 %. Based on the results obtained, 20 ppm dye concentration were chosen to check the maximum photodegradation of MO dye with minimum screening effect.

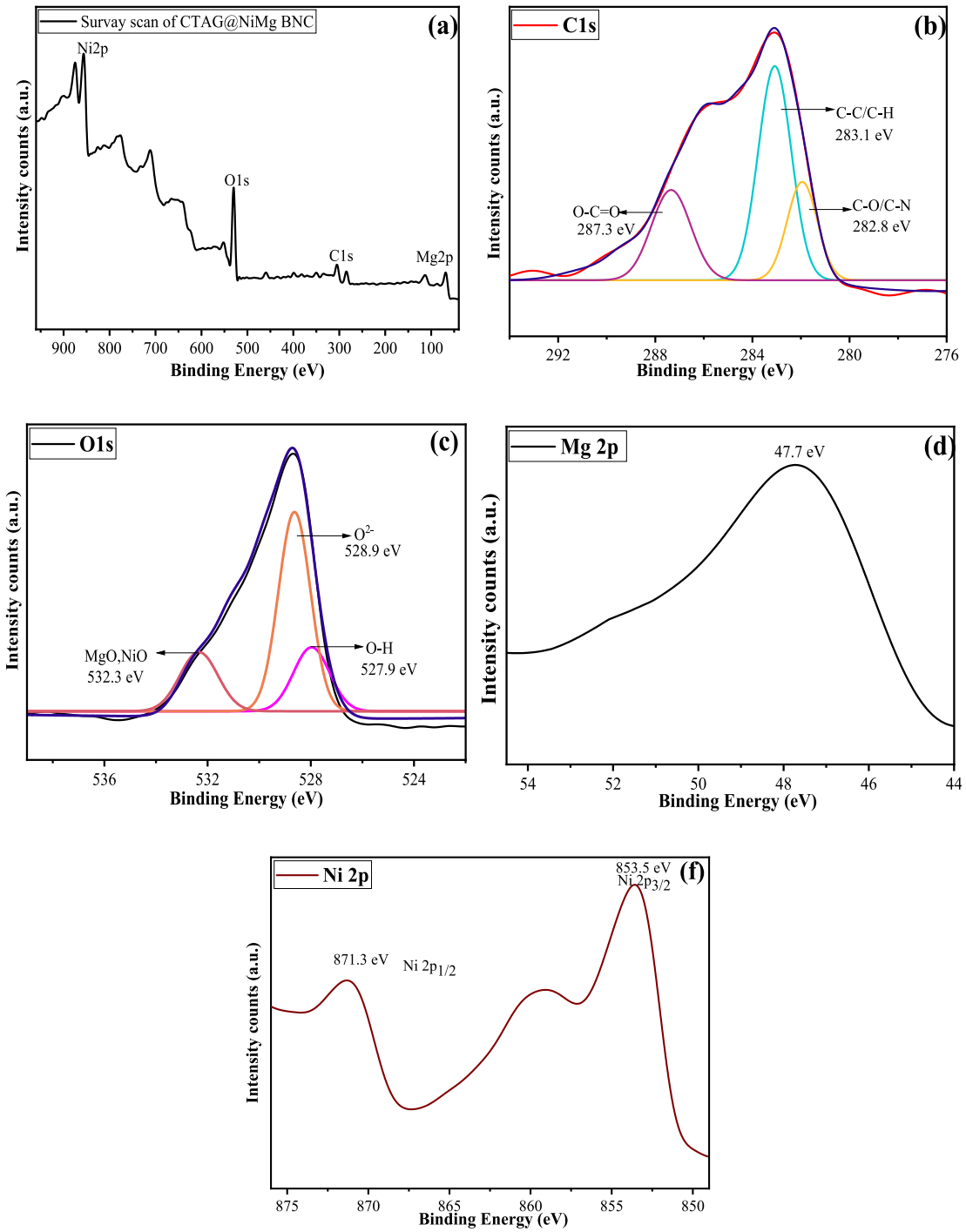

Fig. 7. X-ray photoelectron spectra of (a) Survey spectra of CTAG@NiMg BNC, (b) C1s, (c) O1s, (d) Mg 2p, (e) Mg 2 s and (f) Ni 2p.

3.2.5. *Effect of pH*

The effect of pH of MO was examined at 20 ppm of MO concentrations under same conditions as applied in the above experiments. The photocatalysis process includes the growth of guest molecules on exterior interface of catalyst, in binding pH plays a very important role. Three pH were used to check the degradation one is from acidic medium i.e., 4, second is 7 i.e., neutral and third is 10 i.e., basic for MO degradation at 20 ppm concentrations. The results are given in Fig. 10 (a) which suggest that in acidic medium, the rate of MO degradation was highest (96 %) as compared to degradation rate at pH 7 (88 %) or pH 10 (81 %). Fig. S6 (a–c) constitute the UV–Vis graphs for variation in absorbance values of MO with respect to irradiation time at pH 4, 7 and 10. It can be seen that as the pH increases from 4 to 10, the photocatalytic efficiency decreases from 96 % to 81 % which can be explained based on point of zero charge (pHpzc) value of the material. Fig. S6 (d) constitutes the zeta potential graph which gives the value of pHpzc equal to 3.45 which suggest that at pH < pHpzc, the surface of the material will be positive and pH > pHpzc the surface of the material will be negative. At pH 4, the MO dye will positive charges due to NH_3^+ groups and the surface of the material will be negative which will exert an attractive electrostatic force and thus maximum number of dye molecules can be adsorbed on the surface of the material and results in high photocatalytic efficiency. As the pH value increases, the repulsive forces between sulfonate anions and negative material surface will result in

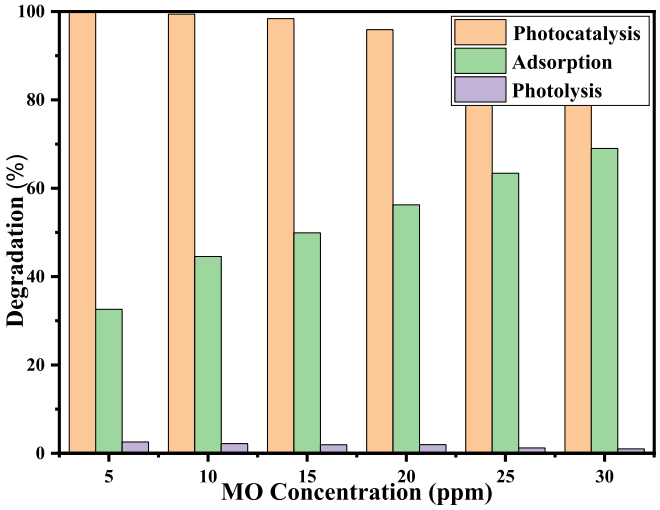

Fig. 8. Bar graph plot of concentration vs % degradation showing leaching effect.

accommodation of a smaller number of dye molecules and hence low photocatalytic efficiency observed at high pH values. Thus pH 4 was chosen as optimum pH for further photocatalytic experiments towards MO degradation.

3.2.6. *Effect of dosage loaded*

The effect of dosage loaded for degradation of MO dye was examined at 20 ppm of MO concentration under same conditions as applied in the above experiments. Fig. S7 (a–c) shows the UV–Vis curve for the MO degradation at 10 mg, 15 mg and 20 mg of dosage respectively and Fig. 10 (b) shows the rate of degradation of MO dye. It was observed that with the increase in dose, degradation of dyes also increases because number of active sites increases and photogenerated hydroxy radicals will help in the photocatalytic degradation of MO dye molecules under visible light. It was found that at maximum % degradation for MO dye was degraded at 20 mg of dose at pH 4 with 20 ppm of MO dye concentration.

3.3. *Scavenger test (Trapping experiment)*

The synthesized material revealed the doping of NiO-MgO matrix and functionalization of CTS-Agar biopolymer matrix which led to the change of band structure of synthesized material which will replicates on the photocatalysis of the synthesized material for MO dye degradation. The reactive oxidant species (ROS) were involved in the photocatalytic degradation of MO in presence of UV light. To clarified which ROS were involved, trapping experiment were performed by taking 25 mL of aliquot of 20 ppm MO at pH 4 with dosage of 20 mg of CTAG@NiMg BNC under UV light. To check the role of specific ROS in degradation of MO, individual aliquot samples were mixed with 3 mM of scavengers like EDTA for h^+, methanol for $OH^\bullet$, ascorbic acid for $O_2^{-\bullet}$ and KI for e^- radical [65–67,76]. Fig. 10 (c) shows the results which suggested that in the presence of EDTA, AA and KI no substantial change takes place in the photocatalytic degradation of MO suggesting there is no contribution of h^+, $O_2^{-\bullet}$ and e^- ROS in the MO degradation. In occurrence of methanol quenched the efficiency from 99.51 % of blank to 78 % suggesting the primary contribution of photogenerated $OH^\bullet$ radical in MO degradation. Mechanism of photocatalytic degradation of MO by CTAG@NiMg BNC material is given below [84]

i. CTAG@NiMg + $h\nu \rightarrow$CTAG@NiMg $(h^+_{VB} + e^-_{CB})$.
ii. CTAG@NiMg (h^+_{VB}) + $H_2O \rightarrow$CTAG@NiMg + H^+ + ·OH.
iii. CTS - Agar@NiO - MgO (e^-_{CB}) + $O_2 \rightarrow$CTAG@NiMg + $\cdot O_2^-$.
iv. $\cdot O_2^- + H^+ \rightarrow HO_2^\cdot$.
v. $CTAG@NiMg(e^-_{CB}) + HO_2^\cdot + H^+ \rightarrow H_2O_2$.
vi. $CTAG@NiMg(e^-_{CB}) + H_2O_2 \rightarrow \cdot OH + OH^-$.
vii. ·OH + MO→Degraded MO.

When the visible light radiations fall on the surface of CTAG@NiMg, the formation of holes and electrons takes place in valence and conduction band respectively. The presence of O_2 will trap the e^- and form superoxide radical $O_2^{-\bullet}$ Which reacts with H^+ ions and form $HO_2^\bullet$ radical equation (iii, iv). The holes (h^+) present on the surface of catalyst will combines with H_2O and form $^\bullet$OH radical, which results in the photocatalytic degradation of MO dye. The attack of $^\bullet$OH radicals on MO dye will convert it into non-toxic products such as CO_2, H_2O and different by products.

3.4. *Influence of water matrix*

Considering the practical application of the synthesized material, it is very important to assess the efficiency in presence of experimental conditions which are close to real ones. Therefore, the photocatalytic degradation of MO dye using CTAG@NiMg BNC were carried out under

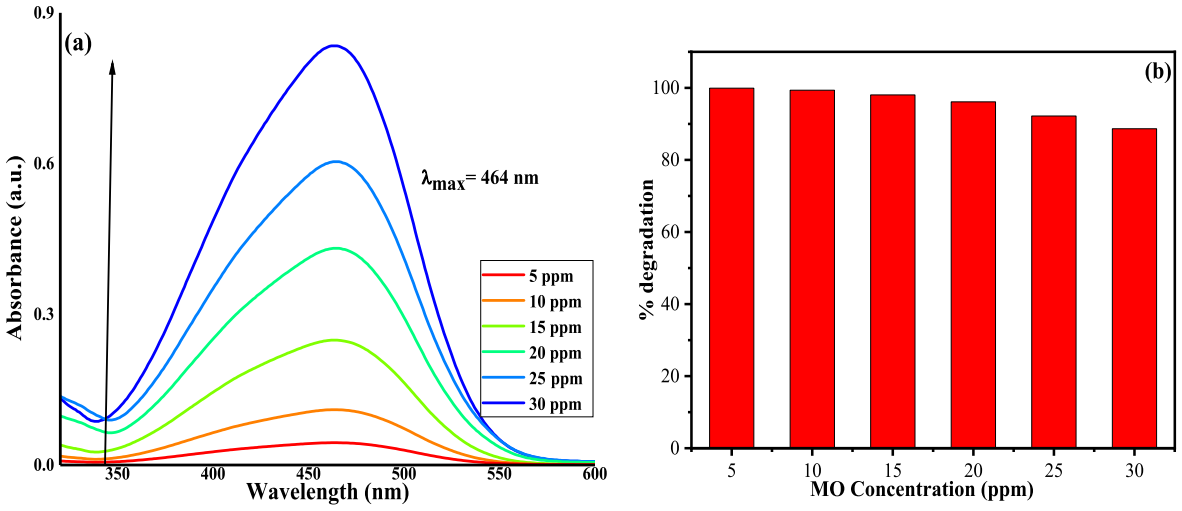

Fig. 9. (a) The effect of different concentration of MO dye (5–30 ppm) by using UV–Vis curve and (b) Bar graph concentration vs %degradation by using 20 mg dose of catalyst under visible light radiation.

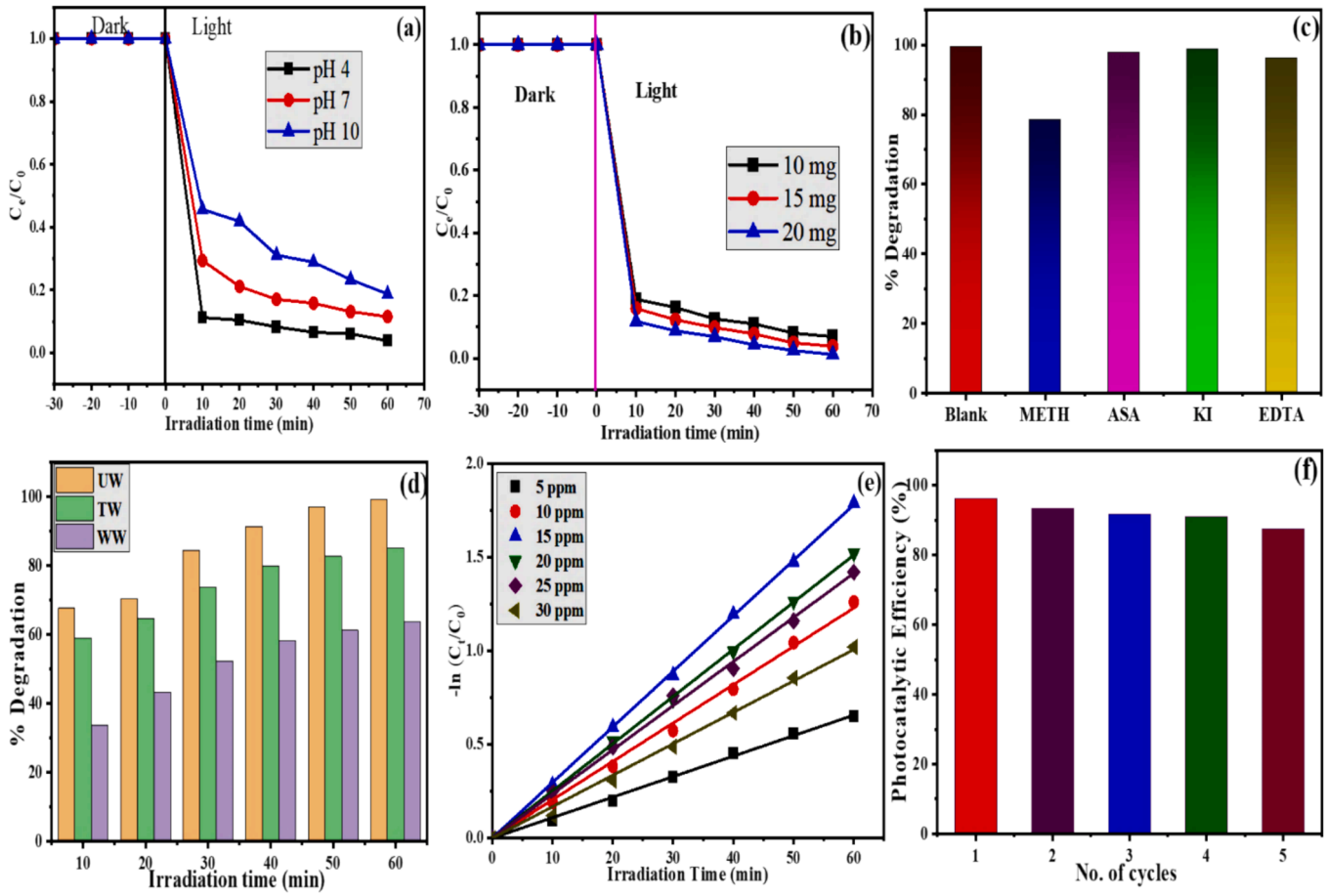

Fig. 10. **(a)** C_e/C_0 graph vs irradiation time (min) for effect of different pH viz 4, 7 and 10 **(b)** C_e/C_0 graph vs irradiation time (min) for effect of catalyst dose viz 10, 15 and 20 mg **(c)** Bar graph of % degradation vs different scavenger for the determination of ROS **(d)** Effect of different water matrix on photocatalysis degradation of MO **(e)** –ln (C_e/C_0) vs irradiation time for 5–30 ppm MO concentration and **(f)** Reusability experiment for CTAG@NiMg BNC (MO concentration = 20 ppm, catalyst dosage = 20 mg, pH = 4, irradiation time = 60 min).

different experimental conditions using different matrix of water i.e., ultrapure water (UW), tap water (TW) and wastewater (WW). The results given in Fig. 10 (d) suggested that in ultra-pure water, the degradation efficiency of MO after 60 min was higher as compared to the other water samples. The results become more pronounced as the complexity of water matrix increases owing to higher amount of natural organic material (NOM) as compared to ultra-pure water (UW) or tap water. The NOM poses a competition towards MO degradation towards consumption of reactive oxidant species such as $^{\bullet}OH$ or $O_2^{\bullet}$ radicals which results in low photocatalytic efficiency for wastewater sample [68]. Whereas, in tap water the inorganic ions act as reactive species scavengers during photocatalysis, which will lead to the formation of different radical spices resulting in low photocatalytic efficiency.

3.5. Kinetics of photodegradation

The photocatalytic degradation of MO dye was examined by CTAG@NiMg BNC for the experiment of irradiation time in the presence of halogen as light source and the type of kinetics will be calculated. At 20 mg of catalyst dose, 10–60 mins of irradiation time at pH 4 at different MO concentration (5–30 ppm) was conclude the pseudo first order reaction. By using given mathematical equation with respect to half-life period was given below [77];

$$-\ln\frac{C_e}{C_0} = kt$$

Table 1
Kinetic parameters for pseudo first order model for MO photodegradation by CTAG@NiMg BNC.

S. N.	MO Conc. (ppm)	Rate constant (k_1) (min^{-1})	Half-life $t_{1/2}$ (min)	R^2
1	5	0.012	56.84	0.99
2	10	0.018	35.38	0.99
3	15	0.021	32.35	0.99
4	20	0.015	44.53	0.99
5	25	0.014	49.26	0.99
6	30	0.016	41.91	0.99

$$t_{1/2} = \frac{0.693}{k}$$

where, C_o and C_e are the initial and final concentration, k_1 is pseudo first order of reaction and $t_{1/2}$ half-life period of reaction.

The kinetic graph of pseudo first order reaction was given in Fig. 10 (e). The first order rate constant (k_1) indicates slope of straight line between $-\ln(C_e/C_0)$ and irradiation time. The values for k_1 are 0.011, 0.022, 0.030, 0.028, 0.026, 0.015 min^{-1} and half-life values are 63.0, 35.6, 25.8, 29.3, 28.7, and 41.7 corresponding to 5, 10, 15, 20, 25, 30 ppm concentration of MO dye respectively for CTAG@NiMg BNC. Table 1 shows a pseudo-order reaction representing R^2 value (0.99) for MO dye concentration which suggest that the kinetic shows the pseudo first order reaction. In this, the MO molecules will accumulate on surface

Table 2
Comparison data of present study with literature.

Material	Light Source	MO concentration (mg/L)	Irradiation time (min)	Catalyst dose (mg)	Degradation (%)	Reference
EGNiO	Florescent lamp	10	90	0.75	96.8	[68]
ZnO	UV	30	10	0.2	99.70	[69]
ZSM-5/ZnO/Ag	UV	5	120	0.07 g	90	[70]
ZnO	Uv	20	180	1.5	92	[71]
Ni-TO_2	UV	50	60	0.7	95.89	[72]
CTAG@NiMg	Halogen	20	60	20 g	99.5	Recent study

of catalyst to establish the equilibrium then photocatalytic degradation of MO initiates under UV light in the presence of $^{\bullet}$OH radicals.

3.6. Reusability of the CTAG@NiMg BNC

Reusability experiments were critical in assessing the economic and environmental sustainability of the CTAG@NiMg bionanocomposite (BNC) during water treatment. After completing each photocatalytic reaction, the catalyst was separated from the reaction mixture by centrifugation, ensuring effective recovery of the material. The collected catalyst was thoroughly washed with distilled water to remove any residual dye or reaction by-products, then dried in an oven before being reused in subsequent photocatalytic experiments. The reusability study was conducted at the optimized conditions: 20 ppm methyl orange (MO) concentration, 20 mg catalyst dose, for 60 min at pH 4 under UV light. The photocatalytic efficiency was evaluated over five consecutive cycles. As shown in Fig. 10(f), the degradation efficiency after the first cycle was 96.14 %, followed by 93.24 % in the second cycle, 91.68 % in the third, 90.88 % in the fourth, and 87.54 % in the fifth cycle. These results indicate that the material maintained high photocatalytic efficiency even after five cycles, confirming its strong potential for repeated use in MO dye degradation under UV light.

3.7. Comparison data

The degradation of methyl orange was compared with the synthesized catalyst under different parameters like pH, concentration, dose load, irradiation time and %degradation. From the Table 2, it was found that the synthesized material CTAG@NiMg BNC was more effective to the photocatalytic degradation of MO dye.

4. Conclusion

The current work explains the synthesis of cost effective and eco-friendly bionanocomposite (BNC) based on the doping of NiO-MgO NPs with chitosan immobilized with agar agar gum. The synthesized material was characterised by using different analytical techniques like FTIR, UV–Vis, XRD, BET, XPS, TEM-SAED and SEM-EDX. The optical analysis reveals the synthesized material is active in both UV and Vis light. Synthesized material was found to be highly sensitive towards the photocatalytic degradation of methyl orange (MO) dye and around 99.52 % of degradation at various optimized reaction conditions viz; 60 min of irradiation time, pH 4, 0.02 g/L of catalyst dose and 20 ppm of MO concentration. The kinetics study showed that photocatalytic degradation of MO possessed pseudo first order rate constant (k_1) values are 0.011, 0.022, 0.030, 0.028, 0.026, 0.015 min^{-1} and half-life time values are 63.0, 35.6, 25.8, 29.3, 28.7, and 41.7 corresponding to 5, 10, 15, 20, 25, and 30 ppm MO dye concentration respectively having R^2 value as 0.99. The trapping experiments showed that hydroxyl OH° radical as primary reactive oxidant species for the degradation of MO in presence of UV radiation Future work is intended to expand the scope by applying the same photocatalysts to a broader range of dyes, including both azo and non-azo dyes like MB, to fully evaluate the versatility and comparative performance of the synthesized bionanocomposites.

CRediT authorship contribution statement

Akshara Bassi: Writing – original draft, Software, Methodology, Investigation, Formal analysis. **Parvathalu Kalakonda:** Writing – review & editing, Validation, Software, Resources, Investigation, Formal analysis, Data curation, Conceptualization. **Imran Hasan:** Writing – review & editing, Visualization, Validation, Supervision, Software, Resources, Project administration, Funding acquisition, Data curation, Conceptualization.

Declaration of competing interest

The authors declare that they have no known competing financial interests or personal relationships that could have appeared to influence the work reported in this paper.

Acknowledgement

The authors extend their thanks to Researchers Supporting Project (Ref: RSPD2024R670), King Saud University, Riyadh, Saudi Arabia.

Appendix A. Supplementary data

Supplementary data to this article can be found online at https://doi.org/10.1016/j.inoche.2024.113499.

Appendix C. Supplementary data

Supplementary data to this article can be found online at https://doi.org/10.1016/j.inoche.2024.113499.

Data availability

The data that support the findings of this study are available from the corresponding author upon reasonable request.

References

[1] P.C. Dey, R. Das, Enhanced Photocatalytic Degradation of Methyl Orange Dye on Interaction with Synthesized Ligand Free CdS Nanocrystals under Visible Light Illumination, Spectrochimica Acta - Part A: Molecular and Biomolecular Spectroscopy 231 (2020) 118122, https://doi.org/10.1016/j.saa.2020.118122.
[2] A.M. Sudapalli, N.G. Shimpi, Tetragonal SnO2 Nanoparticles: An Efficient Photocatalyst for the Degradation of Hazardous Ionic Dyes, ChemistrySelect 8 (1) (2023) e202203310.
[3] M.J. Chatterjee, S.T. Ahamed, M. Mitra, C. Kulsi, A. Mondal, D. Banerjee, Visible-light influenced photocatalytic activity of polyaniline -bismuth selenide composites for the degradation of methyl orange, rhodamine B and malachite green dyes, Appl. Surf. Sci. 470 (2019) 472–483, https://doi.org/10.1016/J.APSUSC.2018.11.085.
[4] R. Shan, Lu. Lili, Gu. Jing, Y. Zhang, H. Yuan, Materials Science in Semiconductor Processing Photocatalytic Degradation of Methyl Orange by Ag / TiO 2 / Biochar Composite Catalysts in Aqueous Solutions, Mater. Sci. Semicond. Process. 114 (2020) 105088, https://doi.org/10.1016/j.mssp.2020.105088.
[5] S. Narendhran, P. Baby Shakila, M. Manikandan, V. Vinoth, P. Rajiv, Spectrochimica Acta Part A: Molecular and Biomolecular Spectroscopy Spectroscopic Investigation on Photocatalytic Degradation of Methyl, Spectrochim. Acta A Mol. Biomol. Spectrosc. 232 (2020) 118164, https://doi.org/10.1016/j.saa.2020.118164.
[6] A.M. Sudapalli, H.M. Chavan, P.M. Badani, N.G. Shimpi, Efficacy of electrospun PAN/g-C3N4 nanofibers as a photocatalyst for the deterioration of hazardous azo

dyes, Opt. Mater. 152 (2024) 115501, https://doi.org/10.1016/J.OPTMAT.2024.115501.
[7] Vu. Quang, T. Khoa, T.-Q. Nguyen, A. Khan, Chemosphere Photocatalytic Degradation of Methyl Orange Dye by Ti 3 C 2 e TiO 2 Heterojunction under Solar Light, Chemosphere 276 (2021) 130154, https://doi.org/10.1016/j.chemosphere.2021.130154.
[8] V. Soni, S. Sonu P., S. Thakur, T. Ahamad, V.H. Nguyen, V. Chaudhary, N. Kumar, S. Kaya, C.M. Hussain, P. Raizada, Oxygen vacancy enriched SrTiO3 and NiO-based S-scheme heterojunction moored on activated carbon from exhausted water filter batteries for ameliorated photodegradation of doxycycline hydrochloride and methyl orange degradation, J. Taiwan Inst. Chem. Eng. 159 (2024) 105419, https://doi.org/10.1016/J.JTICE.2024.105419.
[9] J. Bhadra, H. Parangusan, A. Popelka, M. Lehocky, P. Humpolicek, N. Al-thani, Journal of Environmental Chemical Engineering Electrospun Polystyrene / PANI-Ag Fi Bers for Organic Dye Removal and Antibacterial Application, J. Environ. Chem. Eng. 8 (3) (2020) 103746, https://doi.org/10.1016/j.jece.2020.103746.
[10] A.P. Shah, S. Jain, V.J. Mokale, N.G. Shimpi, High performance visible light photocatalysis of electrospun PAN/ZnO hybrid nanofibers, J. Ind. Eng. Chem. 77 (2019) 154–163, https://doi.org/10.1016/J.JIEC.2019.04.030.
[11] S. Varjani, P. Rakholiya, H.Y. Ng, S. You, J.A. Teixeira, Microbial degradation of dyes: An overview, Bioresour. Technol. 314 (2020) 123728, https://doi.org/10.1016/J.BIORTECH.2020.123728.
[12] Bassi, Akshara, Kushal Qanungo, Imran Hasan, Alanoud Abdullah Alshayiqi, and Alanood Sulaiman Ababtain. 2023. "CuO Nanorods Immobilized Agar-Alginate Biopolymer : A Green Functional Material for Photocatalytic Degradation of Amaranth Dye." 1–21.
[13] A.S. Yusuff, L. Taofeek Popoola, E.I. Aderibigbe, Solar photocatalytic degradation of organic pollutants in textile industry wastewater by ZnO/pumice composite photocatalyst, J. Environ. Chem. Eng. 8 (4) (2020) 103907, https://doi.org/10.1016/J.JECE.2020.103907.
[14] S. Jain, A.P. Shah, N.G. Shimpi, An efficient photocatalytic degradation of organic dyes under visible light using zinc stannate (Zn2SnO4) nanorods prepared by microwave irradiation, Nano-Struct. Nano-Objects 21 (2020) 100410, https://doi.org/10.1016/J.NANOSO.2019.100410.
[15] M. Jha, S. Ansari, N.G. Shimpi, Ultrasonic assisted green synthesis of Ag:CdO nanocubes and nanospheres using Citrus limon leaves for efficient degradation of organic dyes, J. Ind. Eng. Chem. 69 (2019) 269–284, https://doi.org/10.1016/J.JIEC.2018.09.030.
[16] M.S. Khan, P.P. Dhavan, B.L. Jadhav, N.G. Shimpi, Ultrasound-Assisted Green Synthesis of Ag-Decorated ZnO Nanoparticles UsingExcoecaria agallochaLeaf Extract and Evaluation of Their Photocatalytic and Biological Activity, ChemistrySelect 5 (41) (2020) 12660–12671, https://doi.org/10.1002/SLCT.202002905.
[17] I. Hasan, F.H.A. Alharthi, Journal of Photochemistry & Photobiology, A: Chemistry Caffeine-Alginate Immobilized CeTiO 4 Bionanocomposite for Efficient Photocatalytic Degradation of Methylene Blue, J. Photochem. Photobiol. A Chem. 433 (2022) 114126, https://doi.org/10.1016/j.jphotochem.2022.114126.
[18] A.M. Sudapalli, N.G. Shimpi, 3D ZnO sunstar rose nanoflowers morphology with surfactant-assisted reflux exhibit excellent optical properties and photocatalytic activity against hazardous organic dyes, Opt. Mater. 136 (2023) 113391, https://doi.org/10.1016/J.OPTMAT.2022.113391.
[19] A.P. Shah, S. Jain, N.G. Shimpi, Enhanced Photocatalytic Activity of Electrospun PAN/Ag-G NFs Under Solar Irradiation for Effective Degradation of Hazardous Organic Dyes, ChemistrySelect 5 (13) (2020) 3897–3905, https://doi.org/10.1002/SLCT.202000128.
[20] A. George, D. Magimai Antoni, X. Venci, A. Dhayal Raj, A. Albert Irudayaraj, L. Josephine, S. John Sundaram, A.M. Al-mohaimeed, D.A. Al, K. Tse-wei Chen, S. W. Kaviyarasu, W.C. Province, S. Africa, Photocatalytic Effect of CuO Nanoparticles Flower-like 3D Nanostructures under Visible Light Irradiation with the Degradation of Methylene Blue (MB) Dye for Environmental Application, Environ. Res. 203 (2022) 111880, https://doi.org/10.1016/j.envres.2021.111880.
[21] N.S. Pavithra, K.N. Manukumar, R. Viswanatha, G. Nagaraju, Combustion-Derived CuO Nanoparticles: Application Studies on Lithium-Ion Battery and Photocatalytic Activities, Inorg. Chem. Commun. 130 (2021) 108689, https://doi.org/10.1016/j.inoche.2021.108689.
[22] A. Sudapalli, N. Shimpi, Investigation of the Photocatalytic Activity of Electrospun and Surface-Modified PAN/α-FeOOH Nanofibers for the Degradation of Hazardous Azo Dyes, Langmuir 39 (44) (2023) 15517–15534, https://doi.org/10.1021/ACS.LANGMUIR.3C01779/SUPPL_FILE/LA3C01779_SI_001.PDF.
[23] A.M. Sudapalli, N.G. Shimpi, Hierarchical self-assembly of 0D/2D β-Bi2O3 crossandra flower morphology exhibits excellent photocatalytic activity against bromophenol dyes, Opt. Mater. 132 (2022) 112849, https://doi.org/10.1016/J.OPTMAT.2022.112849.
[24] M. Rani, U. Shanker, Photocatalytic Degradation of Toxic Phenols from Water Using Bimetallic Metal Oxide Nanostructures, Colloids Surf A Physicochem Eng Asp 553 (2018) 546–561, https://doi.org/10.1016/j.colsurfa.2018.05.071.
[25] Yu. Shen, Q. Sheng, J. Zheng, A High-Performance Electrochemical Dopamine Sensor Based on a Platinum-Nickel Bimetallic Decorated Poly(Dopamine)-Functionalized Reduced Graphene Oxide Nanocomposite, Anal. Methods 9 (31) (2017) 4566–4573, https://doi.org/10.1039/c7ay00717e.
[26] S. Noor, S. Sajjad, S. Ahmed, K. Leghari, M. Long, Energy Harvesting for Electrochemical OER and Solar Photocatalysis via Dual Functional GO / TiO 2 -NiO Nanocomposite, J. Clean. Prod. 277 (2020) 123280, https://doi.org/10.1016/j.jclepro.2020.123280.
[27] S. Thamri, I. Sta, M. Jlassi, M. Hajji, H. Ezzaouia, Fabrication of ZnO-NiO Nanocomposite Thin Films and Experimental Study of the Effect of the NiO, ZnO Concentration on Its Physical Properties, Mater. Sci. Semicond. Process. 71 (August) (2017) 310–320, https://doi.org/10.1016/j.mssp.2017.08.017.
[28] S. Yasmeen, F. Iqbal, T. Munawar, M.A. Nawaz, M. Asghar, A. Hussain, Synthesis, Structural and Optical Analysis of Surfactant Assisted ZnO–NiO Nanocomposites Prepared by Homogeneous Precipitation Method, Ceram. Int. 45 (14) (2019) 17859–17873, https://doi.org/10.1016/j.ceramint.2019.06.001.
[29] M. Heidarizad, S. Sevinç Şengör, Synthesis of Graphene Oxide/Magnesium Oxide Nanocomposites with High-Rate Adsorption of Methylene Blue, J. Mol. Liq. 224 (2016) 607–617, https://doi.org/10.1016/j.molliq.2016.09.049.
[30] K. Kannan, D. Sivasubramanian, P. Seetharaman, S. Sivaperumal, Structural and Biological Properties with Enhanced Photocatalytic Behaviour of CdO-MgO Nanocomposite by Microwave-Assisted Method, Optik 204 (2020) 164221, https://doi.org/10.1016/j.ijleo.2020.164221.
[31] V. Revathi, K. Karthik, Microwave Assisted CdO–ZnO–MgO Nanocomposite and Its Photocatalytic and Antibacterial Studies, J. Mater. Sci. Mater. Electron. 29 (21) (2018) 18519–18530, https://doi.org/10.1007/s10854-018-9968-1.
[32] K. Selvi, K.A. Tamizh, M.P. Mangai, S. Sagadevan, Investigation of the Dielectric and Impedance Properties of ZnO/MgO Nanocomposite, Phys. B Condens. Matter 594 (2020) 412355, https://doi.org/10.1016/j.physb.2020.412355.
[33] N.A. Alarfaj, M.h.F. El-tohamy, New Functionalized Polymeric Sensor Based NiO / MgO Nanocomposite for Potentiometric Determination of Doxorubicin Hydrochloride in Commercial Injections and Human Plasma, Polymers 12 (12) (2020) 3066, https://doi.org/10.3390/polym12123066.
[34] A.S. Fatesh, R.K. Al, A.H. Fakeeha, S.O. Kasim, J. Khatri, A.A. Ibrahim, R. Arasheed, M. Alabdulsalam, M.S. Lanre, A.I. Osman, A.E. Abasaeed, A. Bagabas, Promotional Effect of Magnesium Oxide for a Stable Nickel - Based Catalyst in Dry Reforming of Methane, Sci. Rep. 1–10 (2020), https://doi.org/10.1038/s41598-020-70930-1.
[35] Z.M. Mizwari, A.A. Oladipo, E. Yilmaz, International Journal of Polymeric Materials and Chitosan / Metal Oxide Nanocomposites: Synthesis, Characterization, and Antibacterial Activity, Int. J. Polym. Mater. Polym. Biomater. (2020) 1–9, https://doi.org/10.1080/00914037.2020.1725753.
[36] A. Aziz, N. Ali, A. Khan, M. Bilal, S. Malik, N. Ali, H. Khan, Chitosan-zinc Sulfide Nanoparticles, Characterization and Their Photocatalytic Degradation Efficiency for Azo Dyes, Int. J. Biol. Macromol. 153 (2020) 502–512, https://doi.org/10.1016/j.ijbiomac.2020.02.310.
[37] A. Khalil, N. Ali, A. Khan, A.M. Asiri, T. Kamal, Catalytic Potential of Cobalt Oxide and Agar Nanocomposite Hydrogel for the Chemical Reduction of Organic Pollutants, Int. J. Biol. Macromol. 164 (2020) 2922–2930, https://doi.org/10.1016/j.ijbiomac.2020.08.140.
[38] T. Sultana, S. Chandra, D. Ashraful, I. Molla, For Adsorption - Assisted Rapid Photodegradation of an Azo Dye in Water, *React. Kinet. Mech. Catal.* (0123456789) (2021), https://doi.org/10.1007/s11144-021-02009-5.
[39] S. Roy, J.W. Rhim, L. Jaiswal, Bioactive Agar-Based Functional Composite Film Incorporated with Copper Sulfide Nanoparticles, Food Hydrocoll. 93 (2019) 156–166, https://doi.org/10.1016/j.foodhyd.2019.02.034.
[40] S. Kumar, J.C. Boro, D. Ray, A. Mukherjee, J. Dutta, Bionanocomposite Films of Agar Incorporated with ZnO Nanoparticles as an Active Packaging Material for Shelf Life Extension of Green Grape, Heliyon 5 (6) (2019) e01867.
[41] N. Karmakar, R. Fernandes, S. Jain, U.V. Patil, N.G. Shimpi, N.V. Bhat, D. C. Kothari, Room temperature NO_2 gas sensing properties of p-toluenesulfonic acid doped silver-polypyrrole nanocomposite, Sens. Actuators B 242 (2017) 118–126, https://doi.org/10.1016/J.SNB.2016.11.039.
[42] S.V.N. Pammi, R. Matangi, S. Ummey, T.R. Gurugubelli, D. Datta, P.N.V.K. Pallela, L.K. Ruddaraju, Photocatalytic, antioxidant, and antibacterial activities of biocompatible MgO flake-like nanostructures created using Piper betle leaf extract, Ceram. Int. 50 (21) (2024) 43248–43254, https://doi.org/10.1016/J.CERAMINT.2024.08.177.
[43] S. Thakur, R. Kumar, Exploration of the structural, optical, and Photocatalytic characteristics of Gd-doped NiO nanoparticles, J. Indian Chem. Soc. 101 (10) (2024) 101255, https://doi.org/10.1016/J.JICS.2024.101255.
[44] R. Vijaya Shanthi, R. Kayalvizhi, M. John Abel, K. Neyvasagam, Analysis on the combined effect of Gd3+ and Er3+ lanthanides in the microscopic, physicochemical and photocatalytic characteristics of MgO nanoparticles, Opt. Mater. 125 (2022) 112118, https://doi.org/10.1016/J.OPTMAT.2022.112118.
[45] S. Ahmadi, S. Ahmad Hivechi, H. Bahrami, P.B. Milan, S.S. Ashraf, Cinnamon Extract Loaded Electrospun Chitosan/Gelatin Membrane with Antibacterial Activity, Int. J. Biol. Macromol. 173 (2021) 580–590.
[46] Y. Wang, A. Pitto-Barry, A. Habtemariam, I. Romero-Canelon, P.J. Sadler, N.P. E. Barry, Nanoparticles of chitosan conjugated to organo-ruthenium complexes, Inorg. Chem. Front. 3 (8) (2016) 1058–1064, https://doi.org/10.1039/C6QI00115G.
[47] Y.A. Arfat, J. Ahmed, H. Jacob, Preparation and Characterization of Agar-Based Nanocomposite Films Reinforced with Bimetallic (Ag-Cu) Alloy Nanoparticles, Carbohydr. Polym. 155 (2017) 382–390, https://doi.org/10.1016/j.carbpol.2016.08.097.
[48] R. Benisha, M. Amalanathan, M. Aravind, M.S.M. Mary, A. Ahmad, S. Tabassum, W.H. Al-Qahtani, I. Ahmad, Catharanthus roseus leaf extract mediated Ag-MgO nanocatalyst for photocatalytic degradation of Congo red dye and their antibacterial activity, J. Mol. Struct. 1262 (2022) 133005, https://doi.org/10.1016/J.MOLSTRUC.2022.133005.
[49] J. Moavi, F. Buazar, M.H. Sayahi, Algal Magnetic Nickel Oxide Nanocatalyst in Accelerated Synthesis of Pyridopyrimidine Derivatives, Sci. Rep. 0123456789 (2021) 1–14, https://doi.org/10.1038/s41598-021-85832-z.
[50] L. Arun, C. Karthikeyan, D. Philip, C. Unni, Journal of Physics and Chemistry of Solids Optical, Magnetic, Electrical, and Chemo-Catalytic Properties of Bio-

Synthesized CuO / NiO Nanocomposites, Journal of Physical and Chemistry of Solids 136 (2020) 109155, https://doi.org/10.1016/j.jpcs.2019.109155.
[51] Obodo, Raphael M., Assumpta C. Nwanya, Muhammad Arshad, Chinedu Iroegbu, Ishaq Ahmad, Rose U. Osuji, Malik Maaza, and Fabian I. Ezema. 2020. "Conjugated NiO-ZnO / GO Nanocomposite Powder for Applications in Supercapacitor Electrodes Material." (October 2019):1–11. doi: 10.1002/er.5091.
[52] A. Ullah, A. Ullah, B. Li, M.H. Mahnashi, B.A. Alyami, Y.S. Alqahtani, A.O. Alqarni, Z. Ul, H. Khan, S. Ullah, M. Wasim, Q. Ullah, W. Ahmad, Photodiagnosis and Photodynamic Therapy Biosynthesis of Silver Capped Magnesium Oxide Nanocomposite Using Olea Cuspidata Leaf Extract and Their Photocatalytic, Antioxidant and Antibacterial Activity, Photodiagn. Photodyn. Ther. 33 (2021) 102153, https://doi.org/10.1016/j.pdpdt.2020.102153.
[53] B. Haspulat Taymaz, V. Eskizeybek, H. Kamış, A novel polyaniline/NiO nanocomposite as a UV and visible-light photocatalyst for complete degradation of the model dyes and the real textile wastewater, Environ. Sci. Pollut. Res. 28 (6) (2021) 6700–6718, https://doi.org/10.1007/S11356-020-10956-0/METRICS.
[54] A. Almontasser, A. Parveen, A. Azam, Synthesis, Characterization and antibacterial activity of Magnesium Oxide (MgO) nanoparticles, IOP Conf. Ser.: Mater. Sci. Eng. 577 (1) (2019) 012051, https://doi.org/10.1088/1757-899X/577/1/012051.
[55] M. Jayapriya, K. Premkumar, M. Arulmozhi, K. Karthikeyan, One-step biological synthesis of cauliflower-like Ag/MgO nanocomposite with antibacterial, anticancer, and catalytic activity towards anthropogenic pollutants, Res. Chem. Intermed. 46 (3) (2020) 1771–1788, https://doi.org/10.1007/S11164-019-04062-1/METRICS.
[56] S. Sadhukhan, A. Bhattacharyya, D. Rana, T. Kumar, J. Tersur, S. Khatua, K. Acharya, D. Chattopadhyay, Synthesis of RGO / NiO Nanocomposites Adopting a Green Approach and Its Photocatalytic and Antibacterial Properties, Mater. Chem. Phys. 247 (2020) 122906, https://doi.org/10.1016/j.matchemphys.2020.122906.
[57] R. Foroutan, S.J. Peighambardoust, H. Aghdasinia, R. Mohammadi, Modification of Bio-Hydroxyapatite Generated from Waste Poultry Bone with MgO for Purifying Methyl Violet-Laden Liquids, Environ. Sci. Pollut. Res. 27 (2020) 44218–44229.
[58] V. Kumar, A. Jain, S. Wadhawan, S.K. Mehta, Synthesis of Biosurfactant-Coated Magnesium Oxide Nanoparticles for Methylene Blue Removal and Selective Pb Sensing, IET Nanobiotechnol. 12 (2018) 241–253, https://doi.org/10.1049/iet-nbt.2017.0118.
[59] J. Mohanta, B. Dey, S. Dey, Sucrose-Triggered, Self-Sustained Combustive Synthesis of Magnetic Nickel Oxide Nanoparticles and E Ffi Cient Removal of Malachite Green from Water, ACS Omega 5 (27) (2020) 16510–16520, https://doi.org/10.1021/acsomega.0c00999.
[60] S. Ye, X. Guan, HMT-Controlled Synthesis of Mesoporous NiO Hierarchical Nanostructures and Their Catalytic Role towards the Thermal Decomposition of Ammonium Perchlorate, Appl. Sci. 9 (2019) 2599, https://doi.org/10.3390/APP9132599.
[61] P. Guerrero, A. Etxabide, I. Leceta, M. Peñalba, K. De La Caba, Extraction of Agar from Gelidium Sesquipedale (Rodhopyta) and Surface Characterization of Agar Based Films, Carbohydr. Polym. 99 (2014) 491–1448, https://doi.org/10.1016/j.carbpol.2013.08.049.
[62] M.A. Ehsan, V. McKee, R. Naeem, A.S. Hakeem, M. Mazhar, Aerosol Assisted Chemical Vapor Deposition of Magnesium Orthotitanate (Mg2TiO4) Films from a Trinuclear Molecular Precursor, Polyhedron 133 (2017) 179–186, https://doi.org/10.1016/j.poly.2017.05.035.
[63] L. Sharma, R. Kakkar, Hierarchical Porous Magnesium Oxide (Hr-MgO) Microspheres for Adsorption of an Organophosphate Pesticide: Kinetics, Isotherm, Thermodynamics, and DFT Studies, ACS Appl. Mater. Interfaces 9 (44) (2017) 38629–38642, https://doi.org/10.1021/acsami.7b14370.
[64] H. Gomaa, E.M. Abd, A.S. El-Monaem, Eltaweil, A.M. Omer, Efficient Removal of Noxious Methylene Blue and Crystal Violet Dyes at Neutral Conditions by Reusable Montmorillonite/NiFe2O4@amine-Functionalized Chitosan Composite, Sci. Rep. 12 (1) (2022) 1–16, https://doi.org/10.1038/s41598-022-19570-1.
[65] B. Mondol, A.M. Anupam Sarker, S.C. Shareque, M.T. Dey, A.K. Islam, S.M. Das, Md. Shamsuddin, A.I. Molla, M. Sarker, Preparation of Activated Carbon/TiO2 Nanohybrids for Photodegradation of Reactive Red-35 Dye Using Sunlight, Photochem 1 (1) (2021) 54–66, https://doi.org/10.3390/photochem1010006.
[66] S.N. Nguyen, T.K. Truong, S.J. You, Y.F. Wang, T.M. Cao, V. Van Pham, Investigation on Photocatalytic Removal of NO under Visible Light over Cr-Doped ZnO Nanoparticles, ACS Omega 4 (7) (2019) 12853–111289, https://doi.org/10.1021/acsomega.9b01628.
[67] M. Pelaez, P. Falaras, V. Likodimos, K. O'Shea, A.A. de la Cruz, S.M. Patrick, J. A. Dunlop Byrne, D.D. Dionysiou, Use of Selected Scavengers for the Determination of NF-TiO2 Reactive Oxygen Species during the Degradation of Microcystin-LR under Visible Light Irradiation, J. Mol. Catal. A Chem. 425 (2016) 183–1119, https://doi.org/10.1016/j.molcata.2016.09.035.
[68] M.F. Hanafi, N. Sapawe, Influence of PH on the Photocatalytic Degradation of Methyl Orange Using Nickel Catalyst, Mater. Today Proc. 31 (2020) 339–341, https://doi.org/10.1016/j.matpr.2020.06.094.
[69] X. Chen, Wu. Zhansheng, D. Liu, Z. Gao, Preparation of ZnO Photocatalyst for the Efficient and Rapid Photocatalytic Degradation of Azo Dyes, Nanoscale Res. Lett. 12 (1) (2017) 4–13, https://doi.org/10.1186/s11671-017-1904-4.
[70] Z. Vaez, V. Javanbakht, Synthesis, Characterization and Photocatalytic Activity of ZSM-5/ZnO Nanocomposite Modified by Ag Nanoparticles for Methyl Orange Degradation, J. Photochem. Photobiol. A Chem. 388 (May) (2020) 112064, https://doi.org/10.1016/j.jphotochem.2019.112064.
[71] Wang, Y., Yang, C., Liu, Y., Fan, Y., Dang, F., Qiu, Y., Zhou, H., Wang, W., & Liu, Y. (2021). Solvothermal Synthesis of ZnO Nanoparticles for Photocatalytic Degradation of Methyl Orange and p-Nitrophenol. *Water 2021, Vol. 13, Page 3224*, *13*(22), 3224. https://doi.org/10.3390/W13223224.
[72] M. Pirsaheb, H. Hossaini, S. Nasseri, N. Azizi, B. Shahmoradi, T. Khosravi, Optimization of Photocatalytic Degradation of Methyl Orange Using Immobilized Scoria-Ni/TiO2 Nanoparticles, Journal of Nanostructure in Chemistry 10 (2) (2020) 143–159, https://doi.org/10.1007/s40097-020-00337-x.
[73] I. Hasan, A. Bassi, K.H. Alharbi, I.I. Binsharfan, Sonophotocatalytic Degradation of Malachite Green by Nanocrystalline Chitosan-Ascorbic Acid @ NiFe 2 O 4 Spinel Ferrite, *Coatings* 10(12):1200 (2020), https://doi.org/10.3390/coatings10121200.
[74] I. Hasan, R.A. Khan, W. Alharbi, K.H. Alharbi, M.A. Khanjer, A. Alslame, Synthesis, Characterization and Photo-Catalytic Activity of Guar-Gum-: G -Aliginate@silver Bionanocomposite Material, RSC Adv. 10 (13) (2020) 7898–7911, https://doi.org/10.1039/d0ra00163e.
[75] I. Hasan, C. Shekhar, W. Alharbi, M.A. Khanjer, Polymers A Highly E Ffi Cient Ag Nanoparticle-Immobilized Alginate-g-Polyacrylonitrile Hybrid Photocatalyst for the Degradation of Nitrophenols, *Polymers* 12(12):3049 (2020), https://doi.org/10.3390/polym12123049.
[76] I. Hasan, C. Shekhar, I.I. Bin, R.A. Sharfan Khan, Ali Alsalme, Ecofriendly Green Synthesis of the ZnO-Doped CuO@Alg Bionanocomposite for Efficient Oxidative Degradation of p-Nitrophenol, ACS Omega 5 (49) (2020) 32011–32022, https://doi.org/10.1021/acsomega.0c04917.
[77] I. Hasan, S. Walia, K.H. Alharbi, M. Abu, A. Alsalme, R. Ahmad, Multi-Walled Carbon Nanotube Coupled β -Cyclodextrin / PANI Hybrid Photocatalyst for Advance Oxidative Degradation of Crystal Violet, J. Mol. Liq. 317 (2020) 114216, https://doi.org/10.1016/j.molliq.2020.114216.
[78] K.D. Khalil, A.H. Bashal, M. Khalafalla, A.A. Zaki, K.D. Khalil, A.H. Bashal, M. Khalafalla, A.A. Zaki, Synthesis, Structural, Dielectric and Optical Properties of Chitosan-MgO Nanocomposite, Journal of Taibah University for Science 14 (1) (2020) 975–983, https://doi.org/10.1080/16583655.2020.1792117.
[79] M. Khan, P. Ware, N. Shimpi, Synthesis of ZnO nanoparticles using peels of Passiflora foetida and study of its activity as an efficient catalyst for the degradation of hazardous organic dye, SN Appl. Sci. 3 (5) (2021) 1–17, https://doi.org/10.1007/S42452-021-04436-4/FIGURES/16.
[80] Khan, M. S., Dhavan, P. P., Ratna, D., & Shimpi, N. G. (2021). Ultrasonic-assisted biosynthesis of ZnO nanoparticles using Sonneratia alba leaf extract and investigation of its photocatalytic and biological activities. *Journal of Cluster Science 2021 33:3*, *33*(3), 1007–1023. https://doi.org/10.1007/S10876-021-02036-1.
[81] Z. Li, Z. Zhang, L. Wang, X. Meng, Bismuth Chromate (Bi 2 CrO 6): A Promising Semiconductor in Photocatalysis, J. Catal. 382 (3) (2020) 40–48, https://doi.org/10.1016/j.jcat.2019.12.001.
[82] M. Rani Rachna, Uma Shanker, Mineralization of Carcinogenic Anthracene and Phenanthrene by Sunlight Active Bimetallic Oxides Nanocomposites, J. Colloid Interface Sci. 555 (2019) 676–688, https://doi.org/10.1016/j.jcis.2019.08.016.
[83] R.K. Shah, Efficient Photocatalytic Degradation of Methyl Orange Dye Using Facilely Synthesized a -Fe 2 O 3 Nanoparticles, Arab. J. Chem. 16 (2) (2022) 104444, https://doi.org/10.1016/j.arabjc.2022.104444.
[84] J. Singh, R.K. Soni, A.g. Zno-cuo, Colloids and Surfaces A: Physicochemical and Engineering Aspects Efficient Charge Separation in Ag Nanoparticles Functionalized ZnO Nanoflakes / CuO Nanoflowers Hybrids for Improved Photocatalytic and SERS Activity, Colloids Surf A Physicochem Eng Asp 626 (2021) 127005, https://doi.org/10.1016/j.colsurfa.2021.127005.
[85] A.M. Sudapalli, N.G. Shimpi, Ag@rGO coral reef morphology exhibits excellent optical properties and photocatalytic activity against methyl orange under sunlight, Diam. Relat. Mater. 139 (2023) 110356, https://doi.org/10.1016/J.DIAMOND.2023.110356.

Dr. Imran Hasan is a distinguished researcher and faculty member at King Saud University, Riyadh. He earned his Ph.D. in applied chemistry from Aligarh Muslim University, India, focusing on the synthesis, characterization, and adsorption properties of nanocomposite materials. His expertise lies in the field of materials science and engineering, with a focus on nanotechnology and its applications in energy and environmental solutions. His current research centers on developing nanocomposite materials for photocatalytic applications, including wastewater purification and green hydrogen production via water splitting. Dr. Hasan is dedicated to advancing research in nanotechnology, with a particular focus on sustainable solutions and the practical application of cutting-edge materials.